Bulletin of the Seismological Society of America, Vol. 98, No. 2, pp. 768–777, April 2008, doi: 10.1785/0120060241

Infrasonic Signals from Large Mining Explosions

by Stephen J. Arrowsmith,* Michael A. H. Hedlin, Brian Stump, and Marie D. Arrowsmith

Abstract We study infrasonic signals from large surface mining explosions in Wyoming. Detections at the Pinedale Infrasound Array (PDIAR) (obtained using a conventional array-processing technique) are automatically associated with ground-truth mining explosions at a range of 368 km. We then focus on four clear signals from mining explosions. By performing a detailed noise study and modeling the propagation of infrasound using a raytracing algorithm and ground-to-space (G2S) atmospheric models, we assess the factors that contribute to the detectability of mining explosions. We find that we can explain most of the observations by propagation and noise effects alone, but that there are at least two notable outliers. Because of high noise levels at the PDIAR array, which places significant constraints on the sizes of mining explosions that can be detected, these results are strongly biased and must be reassessed for lower-noise infrasound arrays.

Introduction

The largest blasts used in surface mining comprise an array of explosions that are detonated in sequence to cast overburden material into an adjacent mine pit. This type of blast typically results in seismic waves that can be observed at regional distances (Stump *et al.*, 2002). With the advent of the international monitoring system in 1996, there has been a drive to develop techniques to identify regional seismic signals. An important element in this scheme is the identification of cast blasts.

In order to fully characterize and identify seismic events, it is advantageous to incorporate data from more than one source. Seismic data rarely provide conclusive evidence for source identification. The complex effect of earth structure between the source and receiver acts as a filter that distorts the source function, complicating the identification process. Also, explosions (in particular, surface mining blasts) can generate seismic waveforms that appear earthquake like (e.g., Arrowsmith *et al.*, 2006). Additional constraints from infrasound have the potential to improve the confidence with which these sources are identified.

Cast blasts result in infrasound signals that can travel distances as large as ~1500 km (Hagerty *et al.*, 2002; Sarker and Kim, 2002; Stump *et al.*, 2004). In contrast, earthquakes, which occur below the surface, are generally less efficient generators of infrasound. This short contribution is a study of infrasonic signals from large mining explosions in Wyoming. We assess the detectability of infrasound signals from ground-truth mining explosions at the Pinedale infrasound array (PDIAR) (located at a range of 368 km from a large-surface coal mine) and comment on the relative effects of ambient noise and atmospheric variability on the detection of mining explosions in this region.

*Present address: Los Alamos National Laboratory, EES-2, P.O. Box 1663, MS D401, Los Alamos, New Mexico 87545.

Detection of Infrasound Signals

We apply an array-based signal detection scheme, the progressive multi-channel correlation (PMCC) algorithm (Cansi, 1995), to the PDIAR data. The basis of the algorithm is a measure of the signal consistency (r_{ijk}) computed between a subnetwork of three proximate array elements (i, j, k), defined by the closure relation

$$r_{ijk} = \Delta t_{ij} + \Delta t_{jk} + \Delta t_{ki}, \tag{1}$$

where Δt_{ij} is the time delay between the arrival of a signal at sensors i and j, computed for each pair of traces using the cross-correlation function. A threshold maximum consistency is defined for the detection of a waveform consistent on all the array elements. If the consistency (r_{ijk}) is less than this threshold, an event is detected on the subnetwork of three array elements. This analysis is performed in a number of separate frequency bands and a series of overlapping windows in time. A nearest-neighbor search method is then used to cluster elementary detections into families associated with individual events by defining maximum allowable variations in time, frequency, azimuth, and velocity for each family. The PMCC algorithm is applied using three filter bands separately: high frequency (1–5 Hz), low frequency (0.1–1 Hz), and very low frequency (0.033–0.1 Hz). The parameters that were chosen for processing the data in the three different bands are given in Table 1 and are based on parameters used by Garces and Hetzer (2002).

Table 1
Parameters Used for the PMCC Processing

Parameter		High Frequency (1–5 Hz)	Low Frequency (0.1–1 Hz)	Very Low Frequency (0.033–0.1 Hz)
Window length (sec)		30	90	300
Window overlap (sec)		5	20	50
Number of frequency bands		10	10	10
Maximum consistency (sec)		0.2	0.5	5
Clustering parameters	Maximum time difference (sec)	10	40	100
	Maximum frequency difference (Hz)	0.8	0.1	0.02
	Maximum azimuth difference (°)	10	10	10
	Maximum speed variation (%)	10	10	10

Dataset

Data for this study come from the four-element PDIAR infrasound array at Pinedale, Wyoming. The array consists of Chaparral II microphones (which have a flat response from 0.1–200 Hz), which are fitted with porous hoses for noise reduction. The porous hoses average acoustic perturbations over a spatial area near the sensor, effectively reducing wind noise while retaining the infrasonic signal of interest (Hedlin *et al.*, 2003). The nominal array element spacing is approximately 100 m (Fig. 1).

We have obtained basic ground-truth information on mining explosions from a large surface coal mine in the Powder River Basin, Wyoming (Fig. 1). The coal mine is located at a range of 368 km from PDIAR. The ground-truth information comprises shot type, location, origin time, and some details about the specific shot configuration and timing sequence. Origin times are typically recorded by the mining engineer responsible for detonating the shot. We have corrected the origin times, which can be inaccurate, using seismic data from the closest available seismic station (RSSD, located in South Dakota at a range of 108 km from the mine). To do this, we search for a waveform at RSSD that occurs at approximately the predicted arrival time (i.e., within ~5–15 min) and exhibits a *Pg-Lg* delay time consistent with the epicentral distance to the mine. The true arrival time is then picked, and a corrected origin time is calculated by ray-tracing through a regional velocity model developed by Prodehl (1979). The corrected origin times are provided in Table 2.

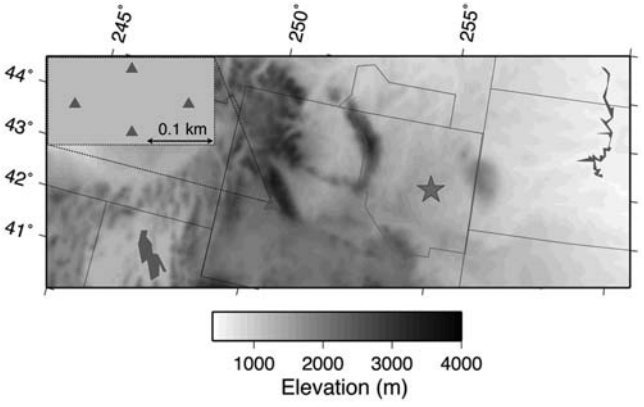

Figure 1. Map showing the locations of the PDIAR infrasound array (triangles) and the surface coal mine from which we have obtained ground-truth data (star). The region enclosed by the black line is the Powder River Basin, a region from which over 350 million tons of coal is mined annually. Inset: blowup of the PDIAR infrasound array.

The complete ground-truth dataset obtained comprises 120 mining explosions, of which 55 are cast blasts. We focus on searching for infrasonic signals from the 55 cast blasts. With the restriction that we require PDIAR array data and a seismic waveform at RSSD for each explosion, the number of cast blasts is reduced to 32 (unfortunately the PDIAR array was temporarily offline at the time of several ground-truth events). For each cast blast, we have obtained 90 min of waveform data (30 min before the corrected origin time; 60 min after).

Noise Characterization

An important component of this study is the assessment of ambient noise amplitudes at the PDIAR array. Ambient noise levels strongly affect our ability to detect signals from mining explosions. To assess the ambient noise levels at the PDIAR array, we have applied the method of McNamara and Buland (2004) to 12 full weeks of data (i.e., 2016 hr of data). We have used data from one week for each month in a year in order to characterize temporal variations in the ambient noise levels. We generate power spectral density (PSD) functions for each 1-hr segment of data (using the processing method described in McNamara and Buland (2004)). Each PSD is then reduced by averaging over 1/8-octave intervals. A probability density function (PDF) of the ambient infrasonic noise is then compiled from the thousands of separate PSDs using the following formula:

$$P(T_c) = \frac{N_{PT_c}}{N_{T_c}},$$

where N_{PTc} is the number of spectral estimates that fall into a 1-dB power bin, with bins ranging from −200 to −80 dB, and T_c is a center period. N_{Tc} is the total number of spectral estimates over all powers with a center period T_c.

Figures 2 and 3 show the PDFs that we obtained of the ambient noise at the PDIAR array. The high-frequency noise floor is ~20 dB above the median infrasound noise model of

Table 2

Summary of Observations and Predictions based on Raytracing

Event #	Origin Time	# Eigenrays	Arrival #	Observed Celerity	Predicted Phase	Predicted Celerity	Observed Trace Velocity	Predicted Trace Velocity	Observed Back Azimuth	Predicted Back Azimuth	# PMCC Detections per Arrival
1	1/8/04 19:23	0	N/A	N/A	N/A	N/A	N/A	N/A	N/A	N/A	N/A
2	2/13/04 19:38	5	N/A	N/A	Iw	0.325	N/A	0.342	N/A	72.9	N/A
					Iw	0.325		0.34		72.6	
					Iw	0.325		0.341		72.6	
					It	0.238		0.347		73.5	
					It	0.239		0.344		73.8	
3	4/4/04 18:30	6	N/A	N/A	It	0.248	N/A	0.345	N/A	72	N/A
					It	0.247		0.342		72	
					It	0.247		0.354		71.7	
					It	0.247		0.347		71.8	
					It	0.247		0.346		72	
					It	0.247		0.341		72	
4	5/18/04 18:22	2	N/A	N/A	Is	0.308	N/A	0.348	N/A	71.9	N/A
					It	0.259		0.392		69.7	
5	5/27/04 18:21	1	N/A	N/A	It	0.261	N/A	0.405	N/A	70.1	N/A
6	5/29/04 18:17	2	N/A	N/A	Is	0.311	N/A	0.367	N/A	71.4	N/A
					It	0.261		0.412		69.4	
7	6/2/04 18:22	2	N/A	N/A	Is	0.31	N/A	0.341	N/A	72.2	N/A
					It	0.262		0.385		69.9	
8	6/5/04 18:20	3	N/A	N/A	Is	0.309	N/A	0.36	N/A	71.6	N/A
					It	0.276		0.603		75.6	
					It	0.263		0.384		70.1	
9	6/7/04 18:23	1	N/A	N/A	It	0.262	N/A	0.404	N/A	69.5	N/A
10	7/7/04 18:04	1	3	0.272	It	0.264	0.366 ± 0.019	0.412	69.5 ± 2.3	69.2	12
11 (*)	7/24/04 19:02	1	1	0.294	It	0.264	0.358 ± 0.014	0.412	67.2 ± 3.9	69.1	35
			2	0.272			0.343 ± 0.014		68.4 ± 3.1		82
12	7/28/04 18:06	2	N/A	N/A	It	0.277	N/A	0.604	N/A	74.2	N/A
					It	0.265		0.41		69.4	
13	7/31/04 20:05	1	N/A	N/A	It	0.264	N/A	0.403	N/A	69.7	N/A
14 (*)	8/2/04 18:03	2	4	0.262	Is	0.312	0.346 ± 0.017	0.359	68.8 ± 3.2	71.7	55
					It	0.262		0.397		69.7	
15 (*)	8/4/04 18:01	1	5	0.291	It	0.262	0.375 ± 0.014	0.395	68.0 ± 3.1	70	62
			6	0.282			0.326 ± 0.022		73.2 ± 2.7		5
			7	0.266			0.342 ± 0.008		69.9 ± 1.1		75
			8	0.265			0.390 ± 0.010		75.7 ± 3.9		6
16 (*)	8/7/04 18:01	2	9	0.292	Is	0.316	0.377 ± 0.016	0.371	65.4 ± 2.9	72.2	6
			10	0.265	It	0.263	0.337 ± 0.006	0.4	67.4 ± 2.7	69.8	5
17	10/9/03 18:08	1	N/A	N/A	It	0.245	N/A	0.349	N/A	72.6	N/A

(*continued*)

Table 2 (*Continued*)

Event #	Origin Time	# Eigenrays	Arrival #	Observed Celerity	Predicted Phase	Predicted Celerity	Observed Trace Velocity	Predicted Trace Velocity	Observed Back Azimuth	Predicted Back Azimuth	# PMCC Detections per Arrival
18	10/13/03 21:00	0	N/A	N/A	N/A	N/A	N/A	N/A	N/A	N/A	N/A
19	10/15/03 20:07	0	N/A	N/A	N/A	N/A	N/A	N/A	N/A	N/A	N/A
20	11/2/03 19:05	0	N/A	N/A	N/A	N/A	N/A	N/A	N/A	N/A	N/A
21	11/3/03 22:15	0	N/A	N/A	N/A	N/A	N/A	N/A	N/A	N/A	N/A
22	11/5/03 21:03	0	N/A	N/A	N/A	N/A	N/A	N/A	N/A	N/A	N/A
23	11/10/03 19:12	0	N/A	N/A	N/A	N/A	N/A	N/A	N/A	N/A	N/A
24	11/19/03 19:06	2	11	0.244	It	0.248	0.362 ± 0.012	0.35	68.6 ± 0.9	74.6	6
					It	0.248		0.358		74.3	
25	11/20/03 19:04	0	N/A	N/A	N/A	N/A	N/A	N/A	N/A	N/A	N/A
26	11/22/03 19:00	0	N/A	N/A	N/A	N/A	N/A	N/A	N/A	N/A	N/A
27	11/24/03 19:03	0	N/A	N/A	N/A	N/A	N/A	N/A	N/A	N/A	N/A
28	11/24/03 21:04	0	N/A	N/A	N/A	N/A	N/A	N/A	N/A	N/A	N/A
29	11/25/03 21:07	0	N/A	N/A	N/A	N/A	N/A	N/A	N/A	N/A	N/A
30	11/26/03 19:00	2	12	0.308	It	0.236	0.396 ± 0.000	0.344	78.6 ± 0.0	73.4	5
					It	0.236		0.348		73.4	
31	12/6/03 19:04	0	N/A	N/A	N/A	N/A	N/A	N/A	N/A	N/A	N/A
32	12/8/03 19:03	0	13	0.272	N/A	N/A	0.308 ± 0.012	N/A	70.7 ± 7.4	N/A	16

The four clear events are labeled with an (*). Note that the phase convention is as follows: Iw is the tropospheric return, Is is the stratospheric return, and It is the thermospheric return.

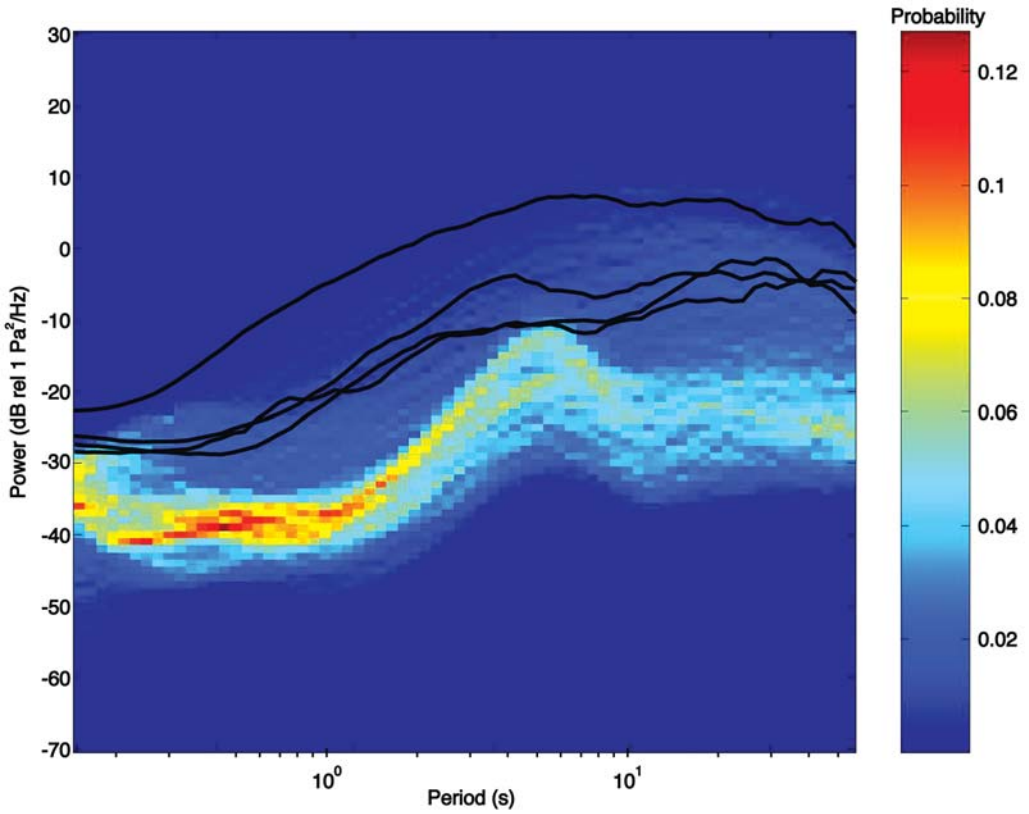

Figure 2. PDF of the ambient power spectral density at the PDIAR infrasound array. Black lines show spectra of signals from the four high-quality mining explosions (see text).

Bowman *et al.* (2005). However, our results agree well with the results of Bowman *et al.* (2005) for the PDIAR array itself. In particular, Bowman *et al.* (2005) observed high levels of noise above 1 Hz at PDIAR, compared with the other infrasound arrays that they studied. A difference between the two sets of results is that we observed approximately 10 dB higher average ambient noise amplitudes in the microbarom band (~0.1–0.5 Hz) during the winter than Bowman *et al.* (2005). However, we note that Bowman *et al.* (2005) surprisingly observed much lower microbarom amplitudes at PDIAR during the winter of 2003 than during 2004, which presumably biased their average estimate. There are two possible reasons for the high ambient noise levels that are observed at PDIAR: (1) high winds at the array location, and (2) instrumentation issues. High noise levels do not appear to be caused by faulty porous hoses, as noise levels are correlated on the individual array components. At lower frequencies, the microbarom peak is clearly apparent (with a peak at 5 sec), degrading the detection of signals in this band. Figure 3 illustrates the temporal variation in noise levels at both diurnal and seasonal time scales. The microbarom energy is greater during the winter months and virtually indistinguishable during the summer. However, the high-frequency ambient noise amplitudes are typically larger during (1) the summer and (2) the middle of the day, which unfortunately corresponds with times when (1) winds are favorable and (2) shots are typically fired. Therefore, the results outlined in the next section should be considered a worst-case scenario for detecting infrasound signals from large mining explosions. If the high-frequency noise floor were more typical (e.g., the median noise model of Bowman *et al.*, 2005), we would expect to detect many more signals. This places significant constraints on what conclusions we can provide in this study about the general effectiveness of infrasound as a monitoring tool.

Infrasonic Signals from Mining Explosions

For each seismically corrected origin time (Table 2), we first apply an automatic search for arrivals (obtained via the PMCC algorithm as described in the previous section) with group velocities (which are simply the total distance divided by the total travel time, and are sometimes termed celerities in the infrasound literature) between 0.22 and 0.34 km/sec and with back-azimuth deviations of ±8°. The range of allowed group velocities is based on typical maximum and minimum group velocities for infrasonic waves (Ceplecha *et al.*, 1998). Typical back-azimuth deviations (i.e., the deviation between the true great-circle back azimuth and the back azimuth of the observed arrival) would be within ±3° (Mutschlecner and Whitaker, 2005), but we allow for a greater range of back-azimuth deviations because there are no clear sources of coherent noise within ±8°. The results of the automatic search for arrivals are shown in Table 2.

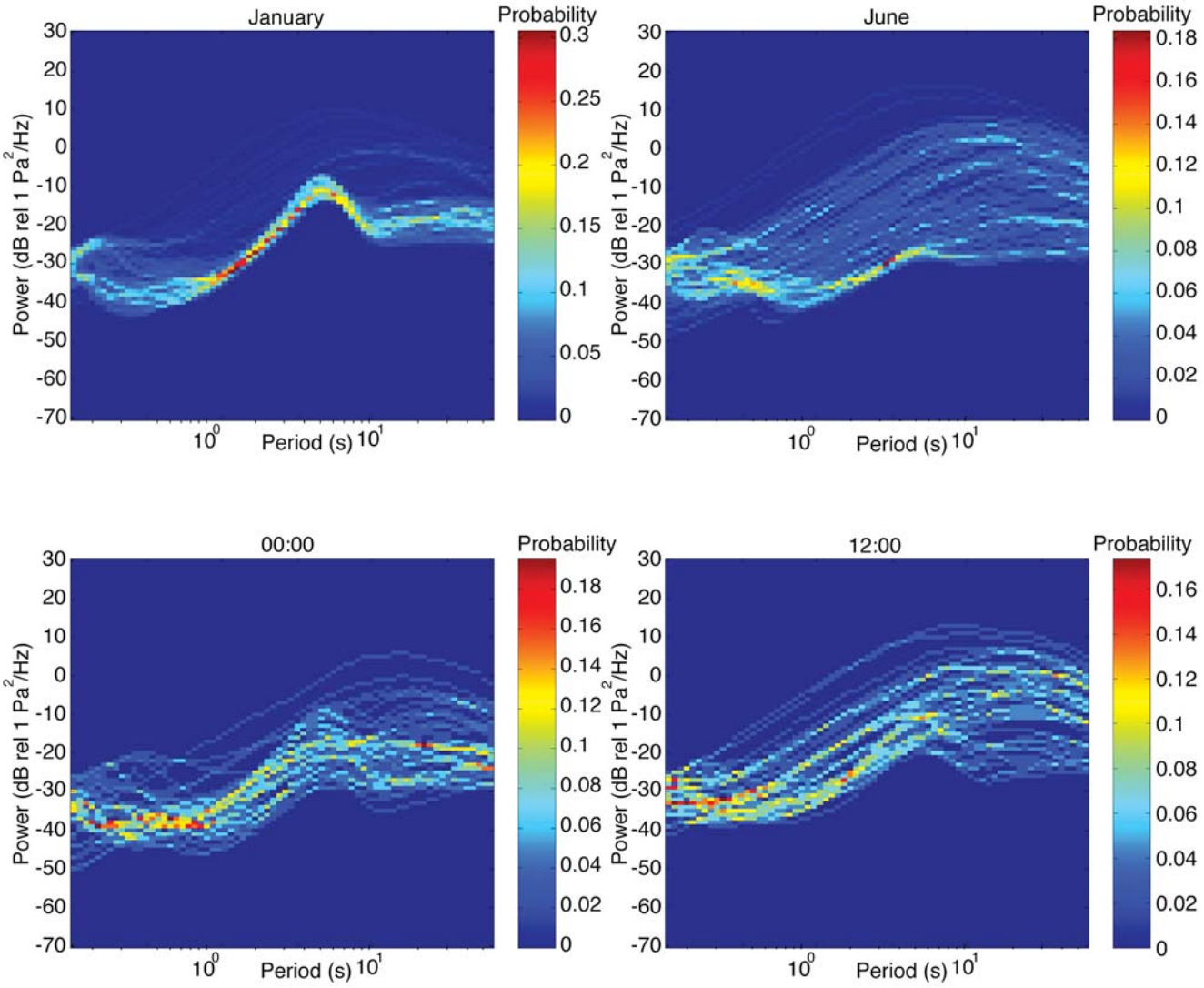

Figure 3. PDFs illustrating the seasonal and diurnal variations in the ambient power spectral density at the PDIAR array. Top panel: PDFs obtained using all waveform data from January (left) and June (right), indicative of winter and summer noise levels, respectively. Bottom panel: PDFs obtained using all waveform data from 00:00–01:00 (left) and 12:00–13:00 (right), where times are in local time.

There were no mining explosions detected in either of the two low-frequency bands, but eight mining explosions were automatically detected in the high-frequency band. We have performed a manual check for visually coherent signals from the undetected explosions and confirmed that PMCC is not missing detections in any of the three frequency bands.

Four events (event numbers 11, 14, 15, and 16; Table 2) are associated with clear signals with signal-to-noise ratios much greater than 1. The remaining four automatically detected events are not clearly visible above the ambient noise level and have therefore been excluded from further analysis to avoid misassociating coherent noise (which can be significant with infrasound data). Beamformed waveforms showing the high-frequency detections from the four clear events are plotted in Figure 4. We note that the four clear signals are all observed during the middle of summer (i.e., July and August).

Averaged spectra for the four high-quality events are plotted in Figure 2 (where each spectrum is averaged over 1/8-octave intervals). The spectra are ~10–20 dB higher than the high-probability ambient noise spectra. However, of particular note, the snapshot preevent noise levels for three of the detected events are unusually low (Fig. 4).

Infrasonic Propagation Modeling

To investigate the effect of atmospheric variability on the observed results, we have modeled the propagation of infrasound using a 3D raytracing routine (Jones *et al.*, 1986). The algorithm accounts for vertical and horizontal refraction as well as horizontal translation of the ray path due to the moving medium. For each ground-truth mining explosion, we have applied an iterative algorithm to search for rays that connect the source to the receiver location within a sphere of 1-km radius. For each subsequent eigenray, we

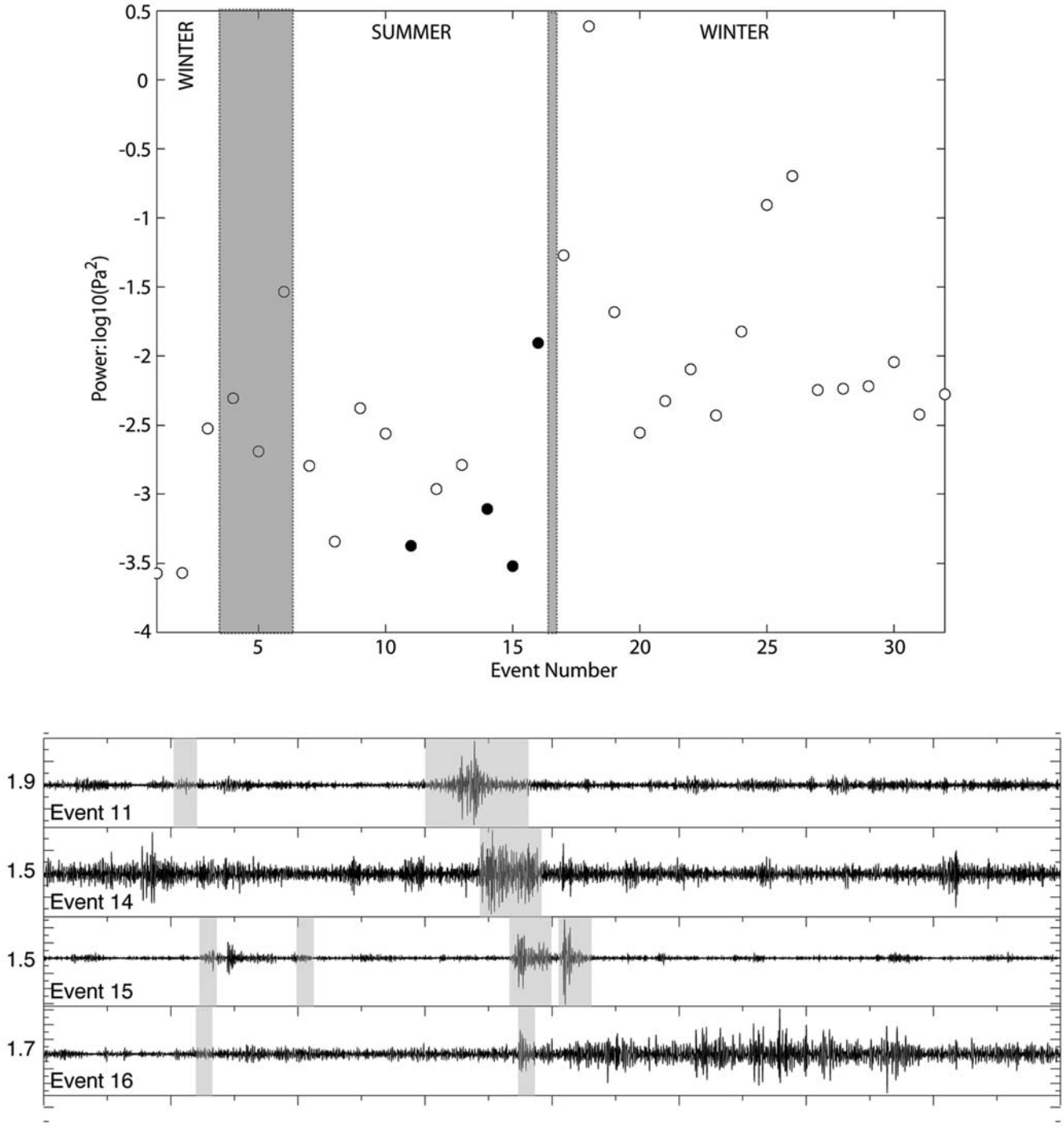

Figure 4. Summary of infrasonic detections from mining explosions. Top panel: Detected shots (solid circles) and undetected shots (open circles) as a function of event number, which increases in relation to time. Gray regions indicate transitional months for stratospheric winds. Bottom panel: Beamformed waveforms for the four clear detections (individual phase arrivals are denoted by shaded gray regions).

obtain a predicted celerity, trace velocity, and back azimuth (Table 2). We utilize the Naval Research Laboratory's ground-to-space (G2S) model, discussed in Drob *et al.* (2003) and Drob (2004), to provide background atmospheric information. The G2S model combines $1° \times 1°$- and $1° \times 1.25°$-resolution global numerical weather prediction (Kanamitsu, 1989; Kalnay *et al.*, 1990) input fields to the nearest 6-hr interval in the lower atmosphere with empirical upper atmosphere models (i.e., the Naval Research Laboratory's mass spectrometer and incoherent scatter radar model [ground to exosphere] 2000 [NRLMSISE-00] and the horizontal wind model 1993 [HWM-93]) (Hedin *et al.*, 1996; Picone *et al.*, 2002) to the nearest universal time hour. The resulting specifications resolve the hourly variation of the upper-

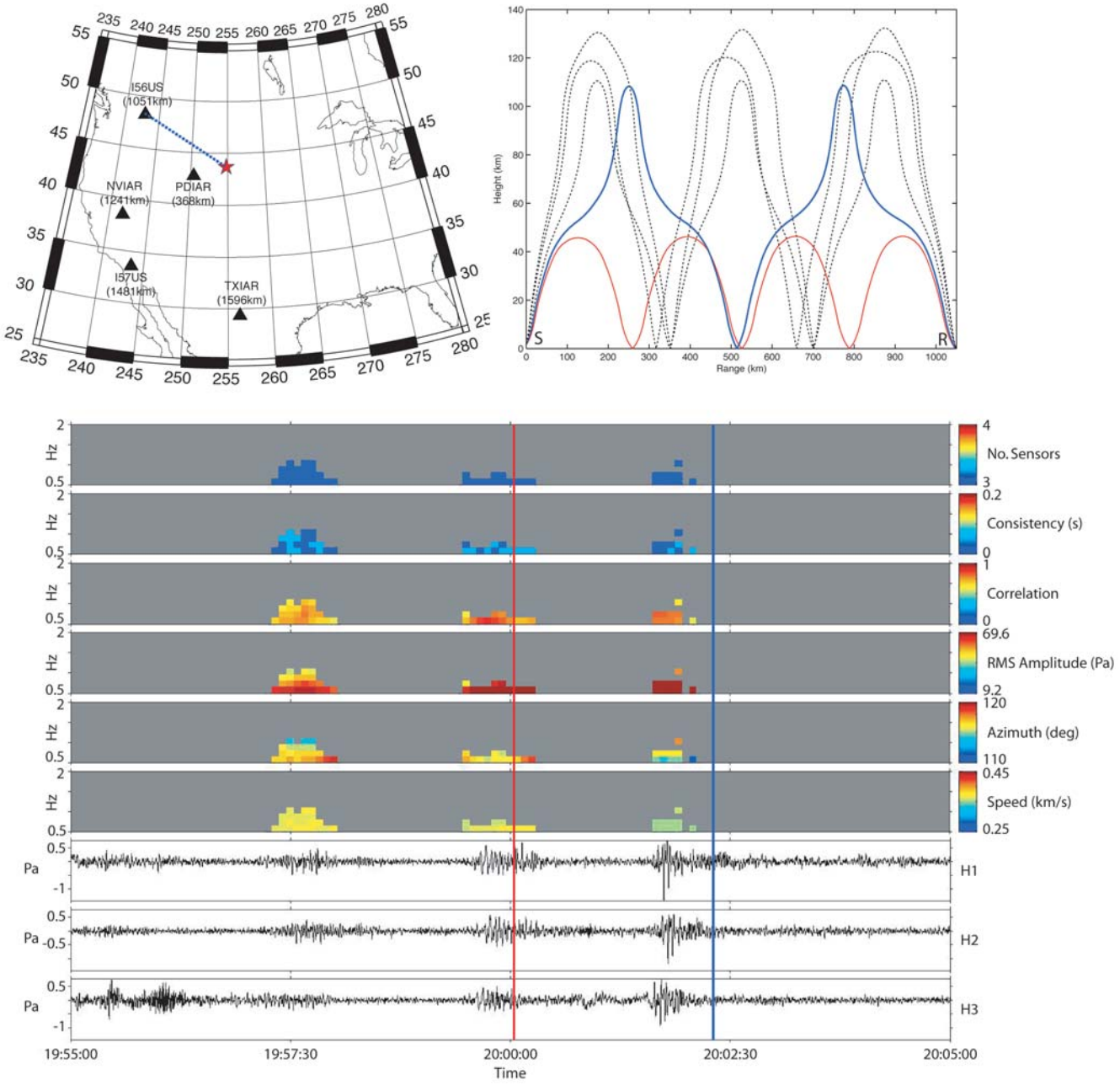

Figure 5. Top left: Locations of all infrasound arrays used in this study (red star denotes the mine location; dashed line shows the propagation path for the observed signal at I56US). Top right: Modeled eigenrays connecting the mine location and the I56US array for signal 11 (Table 2). Bottom: Waveforms and derived parameters of signal 11 recorded at I56US. Vertical red and blue lines show predicted arrival times for the red and blue ray paths shown in the top right panel.

atmospheric solar-migrating tidal components as well as the synoptic meteorology in the troposphere and stratosphere.

The modeling results are provided in Table 2. For each of the four high-quality mining events detected, the ray-tracing algorithm finds between one and two eigenrays that connect the source to the receiver within a miss distance of 1 km. In each case, we obtain a single eigenray that is refracted in the thermosphere, while for events 14 and 16, we obtain an additional eigenray that is refracted in the stratosphere. For each event, there is a good correlation between the latest arrival (also the clearest arrival in each case) and the predicted thermospheric return. However, there is not such a clear correspondence with earlier arrivals and predicted stratospheric returns (except for event 16). For 14 undetected ground-truth events, we did not obtain eigenray solutions; however, we did obtain eigenrays for 13 undetected events (Table 2). In conjunction with the preevent noise study discussed earlier, these results explain a significant number of cases in terms of whether or not we observe detections, although there are other factors that play signifi-

cant roles. In particular, we note that event 8 is associated with low noise and eigenray solutions, but was not detected; in contrast, event 16 is associated with high noise levels but was still detected. An important factor not considered in this study is shot size. Unfortunately, we were unable to obtain detailed information on shot sizes to evaluate this more thoroughly.

Signals at More Distant Infrasound Arrays

There have been relatively few observations of infrasound signals from large mining explosions at distances greater than 1000 km (Christie *et al.*, 2005). Despite this, we have searched for signals from the six clear mining events (as recorded at PDIAR) at four additional infrasound arrays that are located between 1000 and 1600 km from the mine (Fig. 5). The search procedure used was similar to the method described in a previous section for PDIAR, and we used the same three frequency bands of observation: 0.033–0.1, 0.1–1, and 1–5 Hz. We found three signals associated with a single event (event 11) in the high-frequency band at the I56US array (which is the closest array after PDIAR). Event 11 was one of the clearest recorded events at PDIAR.

Using the same method outlined previously, we have performed a raytracing computation for this event to I56US (Fig. 5). We found five eigenrays (one stratospheric [Is] return and four thermospheric [It] returns) that connect the source and receiver within a miss distance of 1 km. The predicted travel times for two rays that fit the observations (one Is and one It return) are also shown in Figure 5. The three remaining eigenrays predict arrivals >5 min after the last observed arrival. The modeled back azimuths of the two matching rays are 116.1° (Is) and 116.2° (It), which correspond remarkably well with the observed back azimuths. It is beyond the scope of this article to undertake a detailed propagation study. However, given the fact that simplifications in propagation physics and atmospheric specifications can lead to appreciable discrepancies between observations and predictions over such a large distance range (1051 km), these modeled data fit with the observational data sufficiently well for the purpose of source identification.

Discussion and Conclusions

We have observed four clear infrasound signals from large mining explosions at the PDIAR array in Wyoming, out of a total of 32 ground-truth cast blast explosions. Although this result may appear disappointing at first glance, the high levels of noise at the PDIAR array imply that the number of detections would likely be much greater if the array conformed to a conventional noise model (Bowman *et al.*, 2005). By modeling the propagation of infrasound using a raytracing algorithm and G2S atmospheric specifications, we show that the observed properties of the four clear events detected at PDIAR are consistent with thermospherically ducted infrasound and with an earlier-arriving stratospheric return in at least one case. We find that variations in atmospheric conditions and noise levels are significant factors that influence the detectability of explosions, but that such variations are themselves insufficient to fully explain the pattern of detections observed. Two outliers of particular note are events 8 and 16 (Table 2 and Fig. 4). However, variations in source properties are also thought to be significant but were not analyzed in this study. Finally, we also searched for signals at more distant infrasonic arrays and found three mining explosion signals at I56US (located at a range of 1051 km), two of which fit predicted eigenrays extremely well.

Acknowledgments

We thank Chris Hayward at Southern Methodist University (SMU) for his valuable insights and suggestions, Rod Whitaker at the Los Alamos National Laboratory (LANL) for providing information on the PDIAR array, and Steve Beil of ArchCoal for providing ground-truth shot-time data. Finally, we thank Keith Koper and two anonymous referees for their constructive reviews on an earlier version of this manuscript. This research was funded by National Nuclear Security Administration Contract Numbers DE-FC52-03NA99510 and DE-FC52-03NA99511.

References

Arrowsmith, S. J., M. D. Arrowsmith, M. A. H. Hedlin, and B. W. Stump (2006). Discrimination of mining events using regional seismic and infrasound waveforms: application to the US and Russia, *28th Seismic Research Review*, Orlando, Florida, 19–21 September 2006.

Bowman, J.-R., G. E. Baker, and M. Bahavar (2005). Ambient infrasound noise, *Geophys. Res. Lett.* **32,** L09803, doi 10.1029/2005GL022486.

Cansi, Y. (1995). An automated seismic event processing for detection and location: the P.M.C.C. method, *Geophys. Res. Lett.* **22,** 1021–1024.

Ceplecha, Z., J. Borovicka, W. G. Elford, D. O. Revelle, R. L. Hawkes, V. Porubcan, and M. Simel (1998). Meteor phenomena and bodies, *Space Sci. Rev.* **84,** 327–471.

Christie, D. R., B. L. N. Kennett, and C. Tarlowski (2005). Detection of regional and distant atmospheric explosions at IMS infrasound stations, *27th Seismic Research Review*, Rancho Mirage, California, 20–22 September 2005.

Drob, D. P. (2004). Atmospheric specifications for infrasound calculations, *InfraMatics* **5,** 6–13.

Drob, D. P., J. M. Picone, and M. A. Garcés (2003). The global morphology of infrasound propagation, *J. Geophys. Res.* **108,** 4680, doi 10.1029/2002JD003307.

Garces, M. A., and C. H. Hetzer (2002). Evaluation of infrasonic detection algorithms, paper presented at the *24th Seismic Research Review*, Ponte Vedra Beach, Florida, 17–19 September 2002.

Hagerty, M. T., W.-Y. Kim, and P. Martysevich (2002). Infrasound detection of large mining blasts in Kazakstan, *Pure Appl. Geophys.* **159,** 1063–0179.

Hedlin, M. A. H., B. Alcoverro, and G. D'Spain (2003). Evaluation of rosette infrasonic noise-reducing spatial filters, *J. Acoust. Soc. Am.* **114,** 1807–1820.

Hedin, A. E., E. L. Fleming, A. H. Manson, F. J. Schmidlin, S. K. Avery, R. R. Clark, S. J. Franke, G. J. Fraser, T. Tsuda, F. Vial, and R. A. Vincent (1996). Empirical wind model for the upper, middle and lower atmosphere, *J. Atmos. Terr. Phys.* **58,** 1421–1447.

Jones, M. J., J. Riley, and T. Georges (1986). GovDoc No. C55.602, A versatile three-dimensional Hamiltonian ray-tracing program for acoustic waves in the atmosphere above irregular terrain, National Oceanic and Atmospheric Administration Special Report, Wave Propagation Laboratory, Boulder, Colorado, 410 pp.

Kalnay, E., M. Kanamitsu, and W. E. Baker (1990). Global numerical weather prediction at the National Meteorological Center, *Bull. Am. Meteorol. Soc.* **71,** 1410–1428.

Kanamitsu, M. (1989). Description of the NMC global data assimilation and forecast system, *Weather Forecast.* **4,** 335–342.

McNamara, D. E., and R. P. Buland (2004). Ambient noise levels in the continental United States, *Bull. Seismol. Soc. Am.* **94,** 1517–1527.

Mutschlecner, J. P., and R. W. Whitaker (2005). Infrasound from earthquakes, *J. Geophys. Res.* **110,** D01108, doi 10.1029/2004JD005067.

Picone, J. M., A. E. Hedin, D. P. Drob, and A. C. Aikin (2002). NRLMSISE-00 empirical model of the atmosphere: statistical comparisons and scientific issues, *J. Geophys. Res.* **107,** no. A12, 1468, doi 10.1029/2002JA009430.

Prodehl, C. (1979). Crustal structure of the western United States, *U.S. Geol. Surv. Profess. Paper 1034*.

Sarker, G., and W.-Y. Kim (2002). Analysis of infrasound signals from Ekibastuz mining blasts at Kurchatov, Kazakstan, paper presented at the *24th Seismic Research Review*, Ponte Vedra Beach, Florida, 2–5 October 2002.

Stump, B. W., M. A. H. Hedlin, D. C. Pearson, and V. Hsu (2002). Characterization of mining explosions at regional distances: implications with the international monitoring system, *Rev. Geophys.* **40,** 1011, doi 10.1029/1998RG000048.

Stump, B., M.-S. Jun, C. Hayward, J.-S. Jeon, I.-Y. Che, K. Thomason, S. M. House, and J. McKenna (2004). Small-aperture seismo-acoustic arrays: design, implementation and utilization, *Bull. Seismol. Soc. Am.* **94,** 220–236.

Institute of Geophysics and Planetary Physics, Scripps Institution of Oceanography
University of California
San Diego, California 92093-0225
sarrowsmith@gmail.com
hedlin@epicenter.ucsd.edu
(S.J.A., M.A.H.H.)

Department of Geological Sciences, Dedman College
Southern Methodist University
P.O. Box 750395
Dallas, Texas 75275-0395
bstump@smu.edu
plutonium@gmail.com
(B.S., M.D.A.)

Manuscript received 16 November 2006